Laser-induced breakdown spectroscopy acoustic testing of the Mars 2020 microphone

Naomi Murdoch, Baptiste Chide, J. Lasue, Alexandre Cadu, Anthony Sournac, Marti Bassas-Portús, X. Jacob, J. Merrison, J.J. J Iversen, C. Moretto, et al.

Laser-induced breakdown spectroscopy acoustic testing of the Mars 2020 microphone

N. Murdoch [a,**], B. Chide [a,b,*], J. Lasue [b], A. Cadu [a], A. Sournac [a], M. Bassas-Portús [a], X. Jacob [c], J. Merrison [d], J.J. Iversen [d], C. Moretto [b], C. Velasco [b], L. Parès [b], A. Hynes [b], V. Godiver [a], R.D. Lorenz [e], P. Cais [f], P. Bernadi [g], S. Maurice [b], R.C. Wiens [h], D. Mimoun [a]

[a] Institut Supérieur de l'Aéronautique et de l'Espace (ISAE-SUPAERO), Université de Toulouse, 31400, Toulouse, France
[b] IRAP-CNRS, Université Toulouse III, 31400, Toulouse, France
[c] Université Toulouse III - Paul Sabatier, Toulouse, France
[d] Department of Physics, University of Aarhus, Denmark
[e] Johns Hopkins University Applied Physics Laboratory, Laurel, MD, 20723, USA
[f] Laboratoire d'Astrophysique de Bordeaux, LAB - UMR, 5804, Bordeaux, France
[g] LESIA, Observatoire de Paris, Meudon, France
[h] Los Alamos National Laboratory, Los Alamos, NM, 87544, USA

Keywords:
Mars 2020
SuperCam
Mars microphone
Laser-induced breakdown spectroscopy
Atmosphere
Soil compaction

A B S T R A C T

The SuperCam instrument suite onboard the Mars 2020 rover will include the Mars Microphone, an experiment designed to record the sounds of the SuperCam laser strikes on rocks and also aeolian noise. In order to record shock waves produced by the laser blasts, the Mars Microphone must be able to record audio signals from 100 Hz to 10 kHz on the surface of Mars, with a sensitivity sufficient to monitor a laser impact at distances up to 4 m. The Aarhus planetary simulator facility has been used to test the Mars 2020 rover microphone in a controlled Martian environment. The end-to-end tests performed in a 6 mbar CO_2 atmosphere, with wind, and also with the microphone at −80° C have demonstrated that the SuperCam/Mars Microphone requirements are satisfied. Tests were also performed on Martian soil simulant targets showing that the variation of the acoustic energy of the shock wave depends on the level of compaction of the target.

1. Introduction

The Mars 2020 mission will launch a rover that will land on, and explore, the surface of Mars between 30° North and 30° South latitude and below 1.0 km elevation as part of the NASA Mars Exploration Program. The SuperCam instrument suite (Wiens et al., 2017) onboard the Mars 2020 rover will include the Mars Microphone (Fig. 1). Its primary purpose is to support the SuperCam Laser Induced Breakdown Spectroscopy (LIBS) investigation of soils and rocks on Mars (Maurice et al., 2015, 2016). As a secondary objective, the Mars Microphone will contribute to basic atmospheric science allowing passive monitoring of the acoustic signals generated by wind and convective vortices interacting with the rover structure.

The Mars Microphone is a commercially available condenser microphone from Knowles Electret. The same technology of microphone has actually flown to Mars twice before: a Knowles Electret EK-3132 on the Mars Polar Lander in 1998 that subsequently crashed onto the red planet (Delory et al., 2007), and a second time, a Gentex 3307-5, in 2007 as part of the Phoenix mission. The microphone was, however, never turned on during the Phoenix mission due to compatibility issues regarding the avionics of the probe (Aeronautics and Administration, 1999).[1] In order to record LIBS shock waves and atmospheric phenomena, the Mars Microphone must be able to record audio signals from 100 Hz to 10 kHz on the surface of Mars, with a sensitivity sufficient to monitor a LIBS blast at distances up to 4 m (typical SuperCam operating distances). This requirement implies a signal to noise ratio of at least 3 dB at 4 m. The Mars Microphone also includes Front-End Electronics with two stages of amplification.

* Corresponding author. Institut Supérieur de l'Aéronautique et de l'Espace (ISAE-SUPAERO), Université de Toulouse, 31400, Toulouse, France.
** Corresponding author.
E-mail addresses: naomi.murdoch@isae.fr (N. Murdoch), baptiste.chide@isae-supaero.fr (B. Chide).

[1] NASA - Mars Descent Imager (MARDI) built by Malin Space Science Systems,URL: https://www.nasa.gov/mission_pages/phoenix/spacecraft/mardi.html.

https://doi.org/10.1016/j.pss.2018.09.009

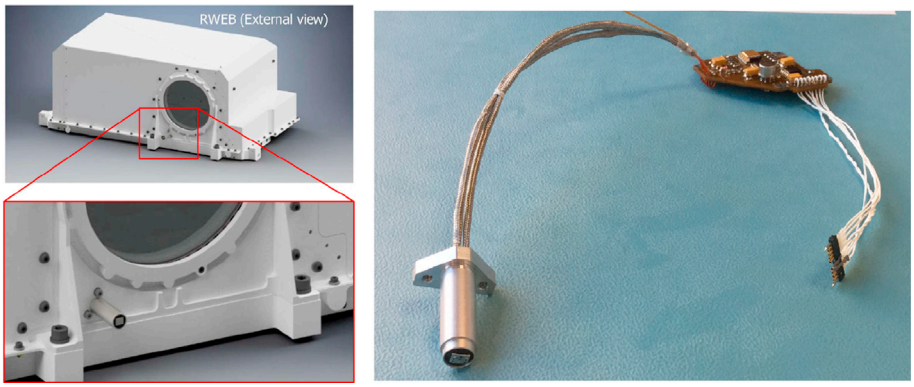

Fig. 1. The accommodation of the Mars Microphone on the SuperCam instrument (left) and the flight model of the Mars Microphone and its Front-End Electronics (right).

However, the environmental conditions at the Martian surface are very different to those found at the surface of Earth: the atmosphere is composed of 96% CO_2 with an average density of 0.02 kg/m^3, the average pressure is ~6 mbar, wind speeds are typically in the order of 5–10 m/s (Murdoch et al., 2017 ; Mimoun et al., 2017), and temperatures at the surface can regularly reach −80° C. The low surface pressure leads to a very small acoustic impedance, and therefore weak coupling of any transducer to the atmosphere. Additionally, molecular absorption by carbon dioxide leads to severe attenuation of the higher acoustic frequencies at the surface of Mars (Williams, 2001). Testing of the Mars Microphone in Mars conditions is, therefore, essential. Additionally, while studies have already been performed at ambient pressure to characterise the laser blast sounds on various rock samples (Maurice et al., 2017), no detailed characterisation has ever been performed under Mars environmental conditions. We have used the Aarhus planetary simulator facility to test four engineering models of the Mars 2020 rover microphone in a controlled Martian environment. Here, we first discuss the findings of previous LIBS acoustic measurements (Section 2). Then we present the test configurations used at the Aarhus planetary simulator facility (Section 3), the results of the end-to-end test of the SuperCam LIBS - Microphone system in the Mars environment (Section 4), and the first detailed characterisation of the LIBS acoustic emission from various Martian soil analogs in the Mars environment (Section 5).

2. Background

Microphones are sometimes used in laser-induced ablation experiments to monitor, in real time, the coupling between the laser and the surface of a sample: the acoustic wave peak-to-peak amplitude variation is dependent on the laser fluence and the surface roughness (Lu et al., 1997). Lu et al., 1997, also outlined different regimes of surface morphology response as a function of the number of pulses: the cleaning of the surface occurs first, then the surface roughening, and finally the ablation of the material. The amplitude response can be predicted with an empirical model. Other experiments used the evolution of the acoustic amplitude as an insight into surface damaging (Diaci and Možina, 1992). By studying the depth of the crater as a function of the number of shots, Grad and Možina, 1993 highlighted a quantitative non linear correlation between the acoustic energy deposited on the crater and the ablation rate.

Conesa et al., 2004 demonstrated the usefulness of LIBS shock wave spectral analysis to give a rapid diagnosis about the plasma formation mechanisms. Palanco and Laserna, 2003 also used the frequency domain of laser induced acoustic emissions to study the influence of the laser irradiance on metallic targets. However, the instrument bandwidth (below 22 kHz) does not allow a precise study of the shock wave as its frequency domain is broad band and centred around 20 kHz (Qin and Attenborough, 2004).

It is recognized that it is hard to get a quantitative analysis with LIBS technique because the plasma spectrum intensity depends on the physical and chemical matrix of the sample targeted (Cremers and Radziemski, 2006). Some studies used the acoustic intensity as a normalisation technique to compensate the shot-to-shot variation in spectra: the minor and major component emission peak area was found to be linearly correlated with the acoustic wave amplitude (Chen and Yeung, 1988), meanwhile the acoustic energy was used to correct for the plasma emission decrease as a function of the number of shots. Unfortunately, this last method does not work for all the wavelengths intervals (Hrdlika et al., 2009). Similarly, Chaleard et al., 1997 used the acoustic intensity, representative of the ablated mass, but also the plasma excitation temperature to provide an analytical model for the plasma emission normalisation. As the shock wave produced by a high energy focused laser pulse incident on a target ("LIBS blast") is indicative of the target's physical properties, the Mars Microphone will help reveal target properties that are otherwise unknown at remote distances.

3. Experiment configuration

The present tests were performed using the Aarhus Wind Tunnel Simulator II [Holstein-Rathlou et al., 2014] in Denmark over one week in July 2017. AWTSII is a climatic chamber housing a recirculating wind tunnel. The cylindrical chamber has a 2.1 m inner diameter, and is 10 m in length. The tests were performed at 6 mbar of 100% of CO_2, achieved by evacuating the chamber and then repressurizing the chamber with CO_2. The facility is fitted with a suite of environment sensors (temperature, pressure, humidity) in addition to an in-situ webcam. The AWTSII chamber is capable of creating Mars atmospheric conditions (including wind) allowing us to test the Mars Microphone in a fully representative environment before flight. The large size of the chamber also ensures that the acoustic measurements can be performed at the required distance of 4 m from the target.

Two different test configurations were used. For the first configuration (Figs. 2 and 3 (a)) two identical microphone benches were installed at distances of ~1.5 m and ~4 m from the laser targets, respectively. The 1.5 m distance corresponds to the anticipated distance between SuperCam and the calibration targets on the Mars 2020 rover, and the 4 m distance corresponds to the distance at which the instrument requirements are defined. For the second test configuration (Figs. 2 and 3(b)), used specifically for the low temperature tests, one microphone was kept at a distance of ~1.5 m from the laser target, two microphones were installed on the cooling plate using a copper support at a distance of ~4 m from the laser target, and the fourth microphone was placed close to the cooling plate at a distance of ~3.8 m from the laser target.

In all of the tests, the chamber was filled with 6 mbar of CO_2 and was kept at ambient temperature. For the low-temperature tests, the cooling plate and the two microphones attached to it were cooled down

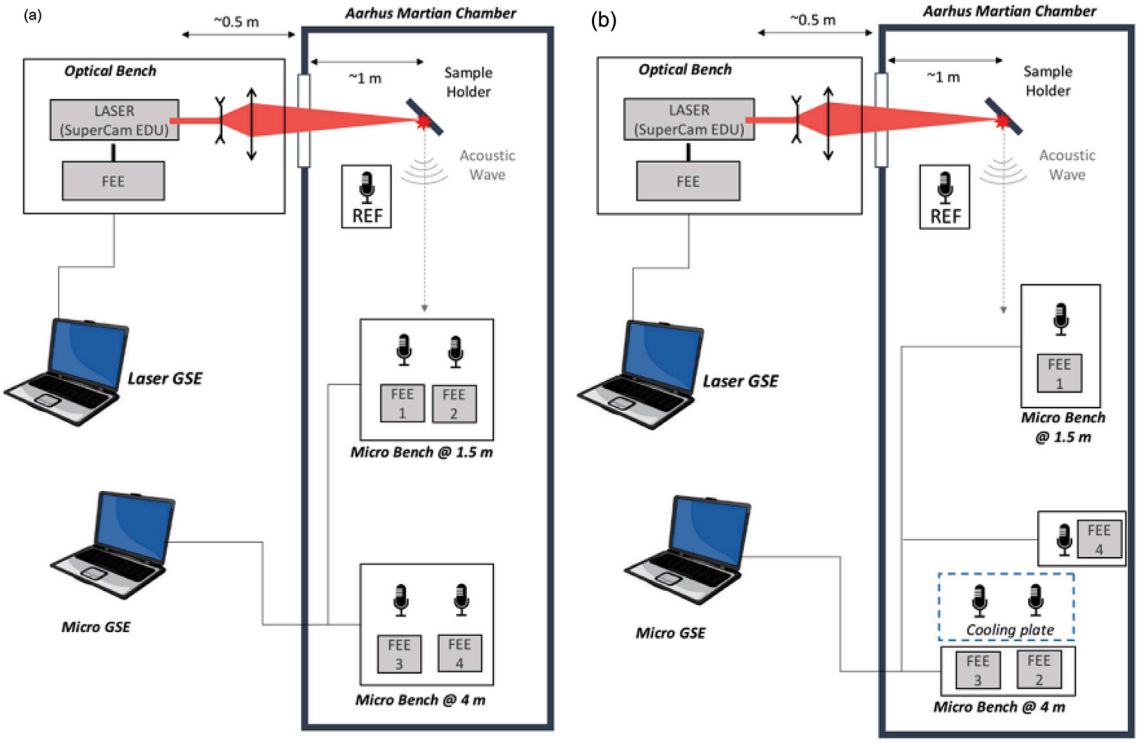

Fig. 2. Schematics of the two test configurations at Aarhus. Left: First test configuration. Right: Second (low-temperature) test configuration. FEE = Front-End Electronics; EDU = Engineering Development Unit; GSE = Ground Support Equipment.

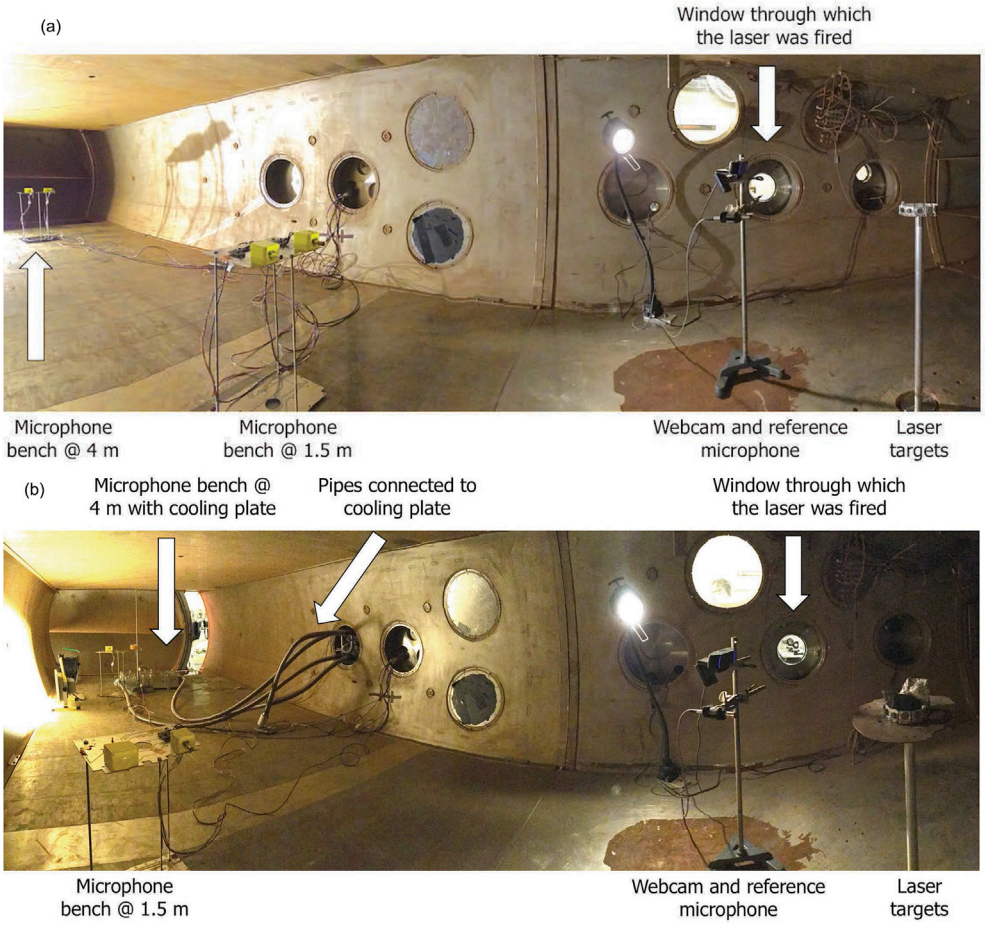

Fig. 3. Panoramic photos of the two test configurations at Aarhus. Above: First test configuration. Below: Second (low-temperature) test configuration.

progressively to −80°C. The electronics were not in contact with the cooling plate and, therefore, were not cooled. These tests were designed specifically to test the microphone performance. Separate, dedicated tests have been performed to verify the performance of the Front-End Electronics at low-temperature.

The specifically designed mechanical interface for the laser targets was a sample wheel capable of holding up to 12 different samples with a 30° separation between them. The sample wheel was attached to a rotating plate inside the wind tunnel (Fig. 4). The sample wheel could then be rotated from outside the chamber allowing the laser impact point to be adjusted on one target, or to change laser target.

3.1. Optical bench

The SuperCam Engineering Development Unit (EDU) laser was used for these tests. The EDU is a Nd:YAG laser with a wavelength of 1064 nm, a 4 ns pulse duration and a laser energy of 25 mJ. The optical bench was located entirely outside the tunnel and the laser was fired through an ISO 200 mm borosilicate (Kodial) glass window, 13 mm thick. Therefore, to obtain the necessary focal length of 1.5 m, a beam expander (Thorlabs BE02-1064) was used in combination with a converging lens (CVI Laser optics PLCX-25.4-772.6-C-1064/532). These optical elements were chosen taking into consideration the fact that the targets are small (cm-sized), that the incidence angle of the laser on the targets is ∼45°, and that the optical elements and chamber window do not have a perfect transmission. Indeed, taking into account the transmission of the optical elements (98% for the beam expander, 99% for the converging lens, 92% for the glass window), the total estimated optical transmission is 89%. Using this information, and the typical spot sizes determined from the impact craters, the laser irradiance and energy on the target are estimated to be 1.5 GW/cm^2 and 22 mJ, respectively.

The laser is fixed on an aluminium plate of roughly 40 by 15 cm mounted on three height adjustable feet. The beam expander and the focus lens are mounted on this same frame. A laser pointer (CPS635F Thorlabs), on a Thorlabs kinematic magnetic mount fixed to the optical bench, was used for the alignment of the optical elements with respect to the targets inside the vacuum chamber. During laser operation, the entire optical bench was covered with a metallic cover for enhanced laser protection, and operators had to wear safety goggles.

In order to align and focus the laser, a LIBS shot was first fired at a large black painted aluminium plate placed at a distance of 1.5 m (the black paint is vaporised by the laser impact thus revealing the raw aluminium below and making it easy to locate the impact point). Then, the alignment of the bench was performed using the laser pointer and the impact point on the target. Once correctly aligned, the optical bench was installed in front of the chamber window and the height of the bench and the laser were manually adjusted. The focus with respect to the laser targets on the sample wheel (Section 3) was then verified by listening to the acoustic signal of the laser impact, which is stronger when the laser is correctly focused. Then, to confirm the alignment for each new target used, a test LIBS shot was fired and a visual inspection was performed via a dedicated porthole to locate the laser impact spot on the target.

The 45° incidence angle of the laser beam on the targets avoided any direct beam reflection into the laser and also allowed us to simulate the typical LIBS analyses as performed on Mars: targets are typically located 2 m away from the rover (horizontally) and are analysed with a LIBS instrument located approximately 2 m from the ground (Maurice et al., 2012).

3.2. Microphone benches

Four engineering models of the Mars Microphones (Knowles Electret model EK-23132) were used during the tests with their respective flight-like Front-End Electronics (FEEs). The sensitivity of the Mars Microphone (and the engineering models) is 22.4 mV/Pa and there are two different stages of amplification gains: the first stage provides an amplification of 16, the second is modifiable at either 2, 4, 16 or 64.

For the first test configuration, the microphones were installed in pairs (in order to have two at 1.5 m and two at 4 m from the target source). Each microphone was fixed to a plastic support that was in turn attached to the Printed Circuit Board (PCB) support made of 1.6 mm thick metalised epoxy. For the second configuration, the microphone that was kept at a distance of ∼1.5 m from the laser target remained attached to the plastic support and PCB support. Two microphones were installed on a cooling plate using a copper support at a distance of ∼4 m from the laser target (see Fig. 5), and the fourth microphone was placed on a mechanical support as close to the cooling plate as possible (at a distance of ∼3.8 m from the laser target). Only the two microphones that were attached to the cooling plate were cooled down. All of the electronics and the other microphones were not thermally coupled to the cooling plate.

In all of the tests there was also a reference microphone (Bruel & Kjaer Cartridge Model 1/2 inch microphone, Type 4165 or Bruel & Kjaer 1/8 inch microphone, Type 4138). The reference microphone was placed

Fig. 4. Laser targets on the specifically designed sample wheel.

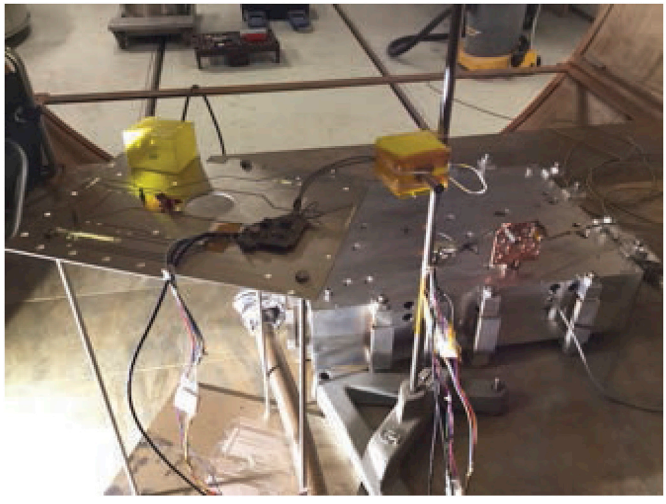

Fig. 5. Photo of the two microphones installed on the cooling plate using a copper support. Another microphone, also seen in the photo, was placed on a mechanical support as close to the cooling place as possible (not thermally coupled). The electronics of this microphone were left attached to the PCB support used during the first test configuration.

close to the laser target (~40 cm) to minimise sound reflections from the walls as previous work (Lorenz et al., 2017) had noted that these are a significant effect in this chamber.

In order to make sure that there is no evidence for acoustic resonances, a comparison was made of the amplitude of a reference sine sweep signal recorded by the microphones at 1.5 m and 4 m. As no frequencies were observed to be significantly amplified, this indicated that no acoustic resonances altered the measurements.

The data acquisition was performed with a datalogger platform (National Instruments PXI platform). The five microphones were sampled simultaneously (and were, therefore, synchronised) at 100 kHz, and a typical data acquisition lasted 20 s.

3.3. Experimental procedures

As the acquisition system limited the recording time to a maximum of 20 s, the laser was programmed to fire 54 times with a frequency of 3 Hz similar to a typical ChemCam measurement sequence (Wiens et al., 2013). This corresponds to 18 s of acquisition and a 1 s margin at the beginning and at the end of the recording. The standard experimental procedure consisted in moving the sample wheel in order to have the desired sample correctly placed, then manually starting the acquisition of the microphones ~1 s before manually starting the laser-firing program. Microphone acquisitions were also regularly performed without the laser being activated in order to quantify the background noise in the experiments: this background noise was significant, due to the fan and the operation of various pumps associated with the chamber.

4. Verification of the Mars Microphone performance requirements

Aluminium reference targets were used in order to verify the microphone performance requirements. Here the results of the acoustic recordings of the LIBS shock waves onto aluminium in Martian conditions are presented.

4.1. Data processing

An example of raw data measured at 1.5 m from an aluminium target is shown in Fig. 6. The acoustic signals corresponding to the 54 LIBS shots can be seen. In order to extract each of the 54 individual peaks of the four Mars Microphones and analyse them separately, the microphones are synchronised with respect to the reference one. Given its close proximity to the laser target and thus the larger amplitude signal, the peaks are first detected in the reference microphone data. Knowing the relative distances of the Mars microphones with respect to the reference microphone, and the estimated sound propagation speed in the tunnel (~280 m/s), it is possible to extract the peaks in the all of the microphones.

Even though the Aarhus chamber is particularly large, there are significant echoes that can be observed in the data (Fig. 7). The first echo to arrive at the microphones situated at 1.5 m from the targets will be the reflection from the lower chamber wall located approximatively 41.5 cm away. It corresponds to an extra distance of ~25.5 cm with regard to the direct wave. Therefore, the first echo will arrive ~9.1 ms after the first arrival assuming a conservative value of 280 m/s for the speed of sound. To avoid complicated data processing techniques to remove the echoes, the expected arrival time of the first echo for each of the microphones is estimated and only the data up until this time is extracted. Unfortunately, the signal length after removing the echoes may be smaller than the real duration of the useful signal.

4.2. Typical acoustic signal

The typical waveforms of the acoustic signals measured at 1.5 m from a LIBS aluminium target are shown in Fig. 8. The waveforms of the

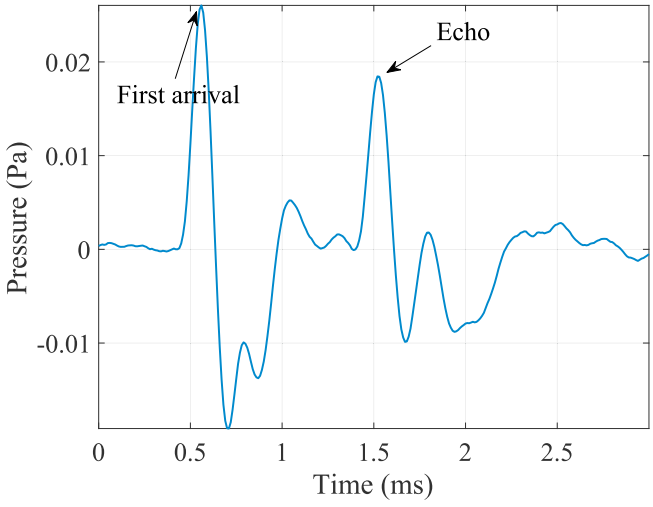

Fig. 7. Acoustic signals of a LIBS shot measured at 1.5 m from a reference aluminium target. The multiple arrivals are due to echoes on the walls of the chamber. The measurements were made with an engineering model of the Mars Microphone.

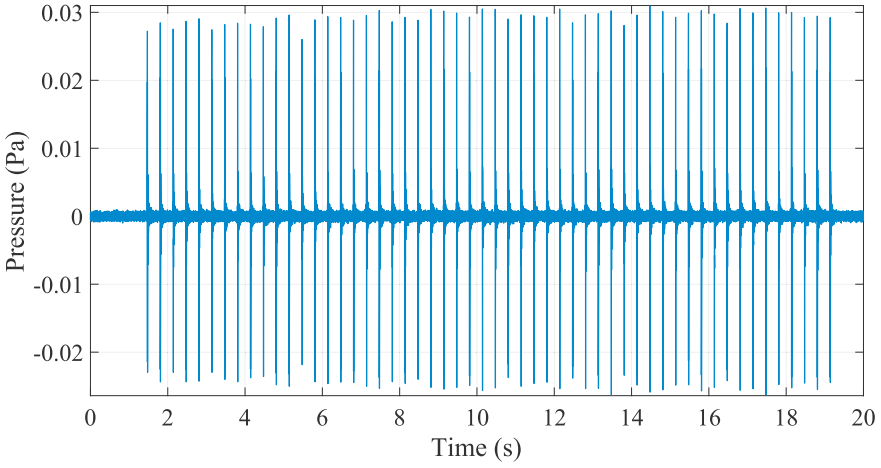

Fig. 6. Acoustic signals of 54 successive LIBS shots measured at 1.5 m from a reference aluminium target in a 6 mbar CO_2 atmosphere. The measurements were made with an engineering model of the Mars Microphone.

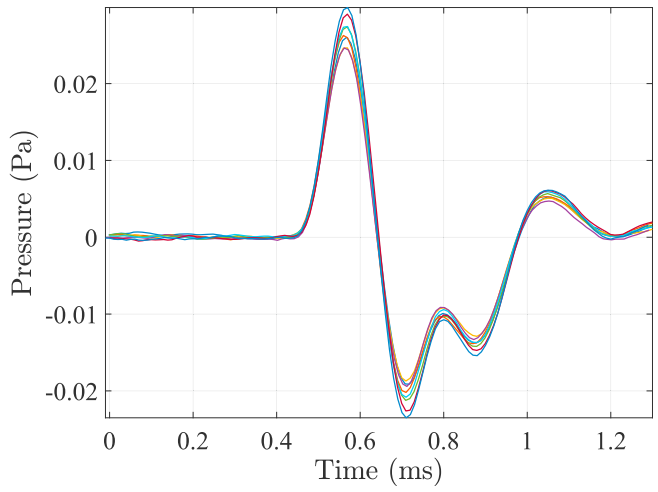

Fig. 8. Typical waveform of a LIBS shot acoustic peak. There are eight lines shown on the figure. Each line represents the acoustic signal from the 25th LIBS shot of a series of 54 shots onto an aluminium target in eight different acquisitions. All data are from tests performed in 6 mbar of CO_2 and measured at 1.5 m from the aluminium laser target.

acoustic wave are very similar for consecutive acquisitions, and are found to have a duration of ~0.8 ms before the first echo. Similarly to previous experiments [e.g., Diaci and Možina, 1992], as the acoustic wave arrives, an initial peak can be seen in the waveform due to the compression of the gas. This is then followed by rarefaction (decompression) resulting in the negative part of the signal. The typical amplitude spectral densities of an entire acquisition (54 shots) can be seen in Fig. 9. The spectra show the bandwidth of the LIBS acoustic signal to be centered around 1 kHz. It appears to be featureless in its bandwidth confirming the shock wave generated by the laser blast as the acoustic source. It can also be seen that the amplitude of both the background noise and the LIBS signals drop off above 10 kHz, as expected due to the strong acoustic attenuation (Williams, 2001).

Signals are also clearly observable in 6 mbar of CO_2 for the aluminium laser target with all four microphone gains (Fig. 10). The SNR of the peak of the acoustic signal is ~38 dB for all four gains. Considering the scaled measurements (Fig. 10, right) the amplitude is seen to increase by ~8% between the highest and lowest amplifications gains. However, this is due to the evolution of the peak amplitude with increasing shot number (see Section 5.4) rather than any influence of the gain (the target was not moved in between these measurements that started in lowest gain and continued to the highest gain).

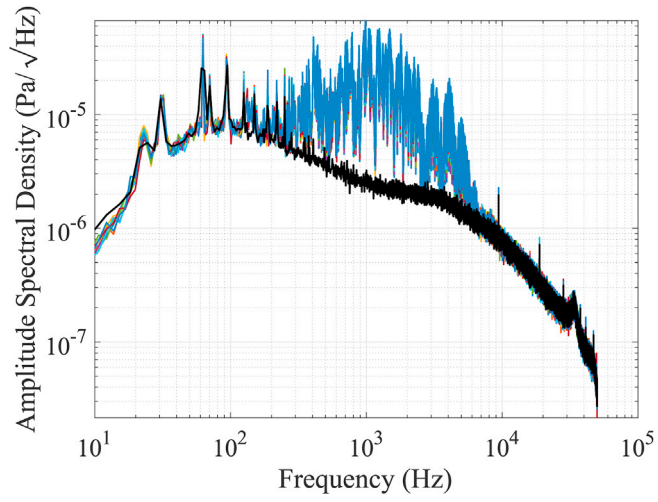

Fig. 9. Typical spectra from a full 20 s acquisition containing 54 successive LIBS shots. Each spectrum corresponds to a different acquisition. The background noise in CO_2 is indicated in black. All data are from tests performed in 6 mbar of CO_2 and measured at 1.5 m from the aluminium laser target. The echoes are not removed from the time series and are, therefore, included in the spectra.

The targets were rotated by hand and, therefore, small variations (a few degrees) from the nominal 45° laser incidence angle may have occurred between tests. A series of dedicated trials were performed in which the laser incidence angle was varied by much more (±10°) than may have occurred accidentally, and such variations were not observed to result in significant changes in the acoustic amplitudes with respect to the nominal 45° incidence angle. A small increase (<2%) observed in peak amplitude when increasing and decreasing the angle of incidence is likely due to the fact that the off-nominal impacts are occurring on a previously un-impacted surface.

4.3. Influence of distance

Fig. 11 shows microphone recordings measured at 1.5 m and 4 m from an aluminium target. By looking for threshold crossing to determine the start of a peak, it was shown that the shock wave travels the 2.5 m separating the two microphones in 9.20 ± 0.02 ms. The sound propagation speed in this configuration is then calculated to be 272.9 ± 0.6 m/s, which is consistent with the estimated speed of sound in carbon dioxide at ambient temperature (Bass and Chambers, 2001). The signal attenuation due to sound propagation can be seen in Fig. 11 and the numerical values for 54 shots are provided in Table 1. For the same gain, the absolute amplitude ratio between the two peaks is equal to 0.11 which is the result of the contribution of two attenuation factors: the geometrical attenuation of the amplitude, due to the propagation of spherical waves, and the contribution of the molecular attenuation due to the propagation of a high frequency content in a 6 mbar CO_2 medium. The sound pressure amplitude p at a distance r from the source is given by:

$$\mathrm{p(r)} = \frac{\mathrm{p_0}}{\mathrm{r}} \mathrm{e}^{-\alpha r} \tag{1}$$

with p_0 being the initial amplitude and α the absorption coefficient in m^{-1}. It is then possible to estimate α in these test conditions by comparing the amplitude at two distances r_1 and r_2 from the source:

$$\alpha = \frac{1}{\mathrm{r_1} - \mathrm{r_2}} \left[\ln(\mathrm{r_2} \times \mathrm{p(r_2)}) - \ln(\mathrm{r_1} \times \mathrm{p(r_1)}) \right] \tag{2}$$

Given the results presented in Table 1, the attenuation coefficient measured between 1.5 m and 4 m is equal to 0.48 m^{-1}. Considering the ~1 kHz frequency characteristic of a LIBS acoustic pulse (see Section 4.2), this value is similar to the predicted attenuation coefficient of 0.32 m^{-1} computed from the model of (Bass and Chambers, 2001) at 293 K for a 6 mbar CO_2 atmosphere with relative humidity of 0.88%. However, the LIBS acoustic signal is not just at 1 kHz and extends over a larger range, from 500 Hz to 6 kHz (see Fig. 9). Over this range, the predicted attenuation coefficient is from 0.20 m^{-1} to 0.50 m^{-1} which explains the slight difference between the experimental value and the attenuation coefficient at 1 kHz.

Despite the high, but expected signal attenuation, the acoustic signals are found to be clearly recordable in 6 mbar of CO_2 for the aluminium laser target at distances of both 1.5 and 4 m.

4.4. Tests with wind

Based on an analysis of Viking Lander 2 in-situ wind data, the mean daytime wind on Mars is expected to be ~3.5 m/s and 70% of the time the wind is expected to be < 4.5 m/s (Mimoun et al., 2007). The background noise during the wind tests (Fig. 12, left) is both a combination of the wind noise on the microphone (as we will have on Mars and which is dominated by low-frequency signals; Lorenz et al., 2017) and the

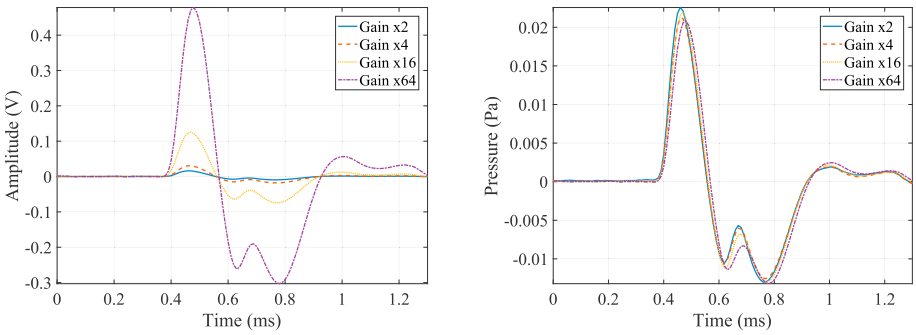

Fig. 10. Influence of the microphone second stage amplification gain. Acoustic measurements of a LIBS shot onto an aluminium target at a distance of 1.5 m in 6 mbar CO_2 atmosphere. The waveforms shown are the mean waveforms of 54 LIBS shots. (Left) The raw microphone data. (Right) The scaled microphone data correcting for the gain and the microphone sensitivity.

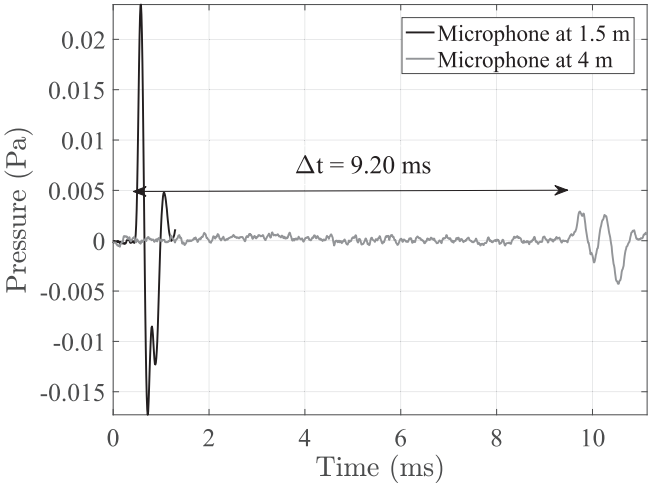

Fig. 11. Signal comparison at different target - microphone distances. Waveforms of the acoustic signal of one LIBS shot on the reference aluminium target as measured by microphones at 1.5 m and 4 m from the target in 6 mbar of CO_2. The signal from the microphone at 1.5 m is the same than in Fig. 7 but it is cut before the first echo arrives.

Table 1
Signal comparison at different target - microphone distances. Measurement data are provided for a microphone at 1.5 m and a microphone at 4 m from the laser target. The laser target is aluminium and the tests were performed in 6 mbar of CO_2 at ambient temperature. The table give the mean results for 54 LIBS shots. The SNR_{rms} is the ratio of the RMS signal to the RMS noise, whereas the SNR_{peak} is the ratio of the maximum signal amplitude to the RMS noise.

Parameter	Microphone at 1.5 m	Microphone at 4 m
RMS noise (Pa)	2.4×10^{-4}	2.7×10^{-4}
RMS signal over 20 ms (Pa)	25×10^{-4}	13×10^{-4}
Peak signal (Pa)	255×10^{-4}	29×10^{-4}
SNR_{rms}	10.2 (20 dB)	4.6 (13 dB)
SNR_{peak}	106.3 (40 dB)	10.6 (21 dB)

mechanical noise of the fan. As the combined wind and mechanical noise dominates at much lower frequencies than the LIBS signal (<1 kHz), a high pass filter is applied to the data to filter out the lower frequency noise (Fig. 12, right). After filtering, the individual LIBS peaks are clearly observable with a mean SNR_{peak} of 28 dB (Fig. 13) at 1.5 m from the laser target, and ~19 dB at 4 m from the laser target.

4.5. Tests at low temperature

As described in Section 3.2, a cooling plate was used in order to also perform tests with the microphones at cold temperature. These tests were designed in order to validate the Mars Microphone requirement of being able to clearly detect the LIBS signal at a distance of ~4 m from the laser target in a Martian atmosphere with a microphone temperature of −80° C. It was demonstrated that the microphone met this requirement with a SNR_{peak} of ~26 dB for individual LIBS peaks, and ~44 dB for the stacked (mean) waveform.

5. Variation of the acoustic signal with target hardness

Section 2 illustrated how the shock wave parameters can give insights into the physical characteristics of the matrix of the sample. In this section, the variation of the LIBS blast acoustic signal is studied as a function of the shot number on seven targets of Martian soil analogue powders with increasing levels of compaction and hardness.

5.1. JSC-1 targets

The Johnson Space Center Mars 1 (JSC1) is a Martian soil analogue composed of Hawaiian volcanic ash particles. It is used on Earth to reproduce the main properties of the Martian regolith such as grain size, density and mineralogy (Allen et al., 1998).

Seven compacted JSC1 powder pellets were prepared for the experiment using a hydraulic press. The compaction level of the targets ranges from 2 tonnes to 15 tonnes which corresponds to a compaction pressure ranging from 0.15 GPa to 1.10 GPa. The targets are cylindrical with a diameter of 13.1 mm and a height varying from 1.0 mm to 2.5 mm.

Vickers hardness measurements were performed on the seven JSC1 targets described above with a Micro Vickers Hardness Tester (Buelher MVK_H1). A pyramidal square-based diamond indenter is pressed on the sample with a load varying from 10 g to 1 kg. The applied load and the size of the indenter footprint give the Vickers Hardness number of the analyzed sample (Bckle, 1959).

The evolution of the mean Vickers Hardness number as a function of the compaction of the target is represented in Fig. 14. Because of the varying grain sizes within each of these compacted grain targets, the dispersion between two successive measurements varies from 2% to 43% for the targets. The hardness is observed to increase for the less compacted targets up to 6 tonnes of compaction and then seems to reach a saturation for the most compacted targets.

5.2. Waveforms of JSC-1 targets

The acoustic waveforms for LIBS shots onto the compacted JSC1 targets are presented in Fig. 15. Although the shape of the waveform is similar to the waveforms produced by laser blast onto the aluminium target (see Fig. 6) the peak amplitude is ~10 mPa lower for the JSC1 samples than for the aluminium target.

Fig. 15 shows that the peak acoustic amplitude increases with target

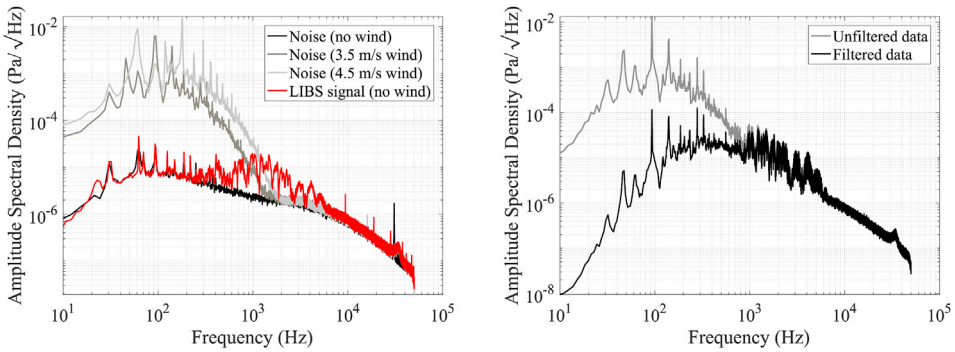

Fig. 12. Frequency content of the wind and LIBS signals. (Left) The amplitude spectral densities of the background noise in the tunnel (black), the noise with a wind of 3.5 m/s (dark grey), the noise with a wind of 4.5 m/s (light grey), and the LIBS signal with no wind present (red). (Right) The amplitude spectral densities of the LIBS signal with background wind at 3.5 m/s before (dark grey) and after (black) filtering of the signal. (For interpretation of the references to colour in this figure legend, the reader is referred to the Web version of this article.)

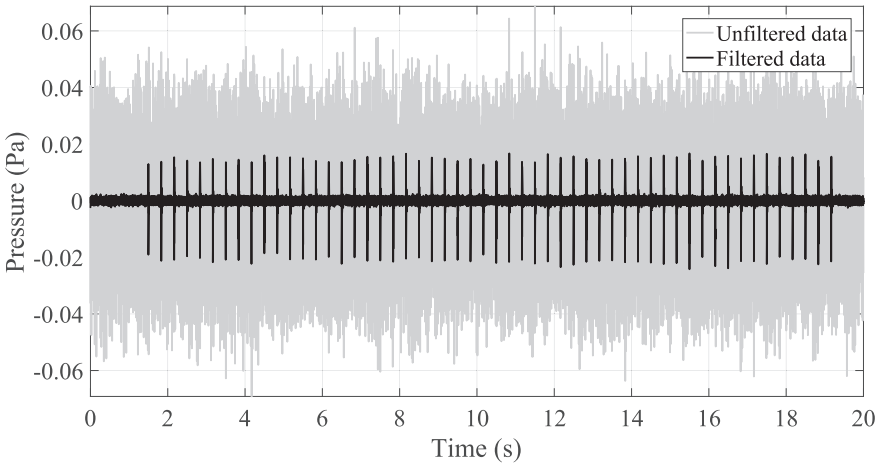

Fig. 13. Time series containing 54 LIBS successive shots with background wind at 3.5 m/s before (grey) and after (black) filtering of the signal.

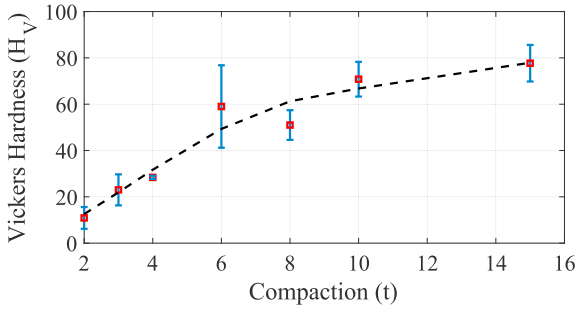

Fig. 14. Vickers Hardness number as a function of the compaction of the JSC1 targets. The error bars give the standard deviation of the five measurements performed on each target.

compaction up to a level of compaction of 6 tonnes. For the higher levels, the amplitude remains constant. This behaviour follows the variation of the Vickers Hardness indicating that the hardness is a critical parameter influencing the acoustic signal.

5.3. Analysis of the target craters

The resulting JSC-1 impact craters were analyzed with a microscope (Olympus GX 71, magnification factor x100) and the pictures are represented in Fig. 16. The average dimension of the crater in the direction of the laser beam is 828 ± 23 µm. There is no significant change in resulting crater diameter with the target compaction (< 3%). Unfortunately, the 45° laser impact angle makes optical profile measurements complicated and it is, therefore, not possible estimate further geometric

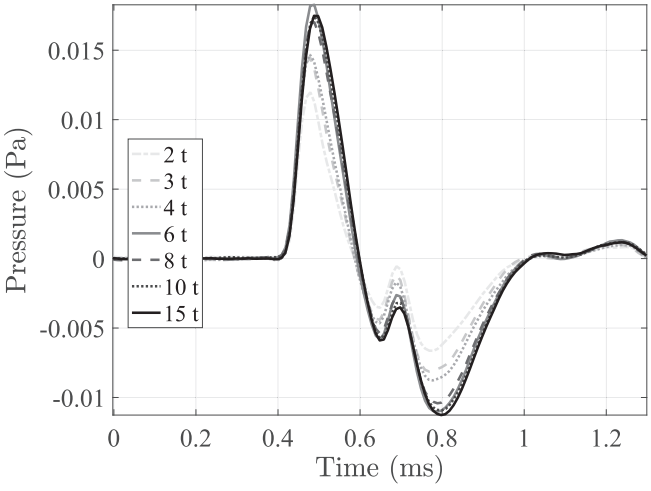

Fig. 15. Waveforms of the acoustic signal from a LIBS shot onto JSC1 targets at different levels of compaction as measured by the microphone at 1.5 m from the targets. Each line represents the average signal over 10 LIBS shots around the 300th shot of the acquisition.

parameters of the craters such as the depth or the ablated volume. This will be the subject of future experiments.

5.4. Signal energy variation with increasing shot number

Here the evolution of the acoustic energy is studied during 432 successive LIBS shots (8 acquisitions of 54 shots) on the same location on a

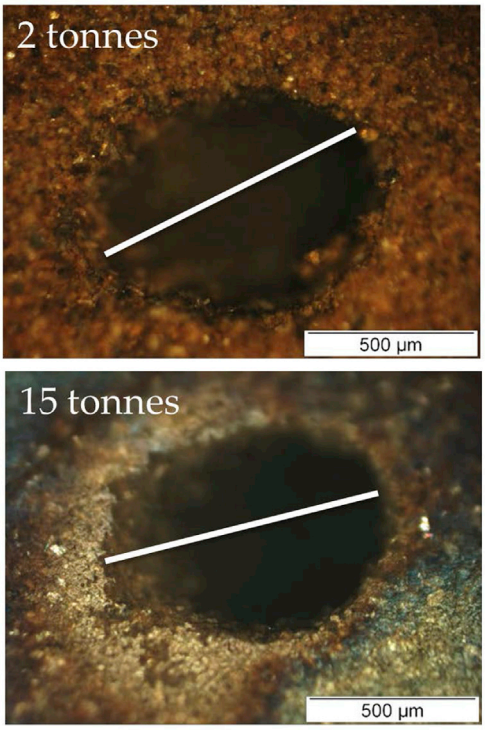

Fig. 16. Microscope images (x100) of impact craters formed via 432 successive LIBS shots (8 acquisitions of 54 shots) on JSC1 targets compacted with a load of 2 tonnes (above) and 15 tonnes (below). The measurement was performed in the direction of the laser beam, as represented by the white line.

JSC1 target. The acoustic energy - the integral of the square value of the acoustic signal from the beginning of the acquisition to the time of arrival of the first echo (i.e., time window of integration is 1.3 ms, see Section 4.1) - is given as a function of the shot number in Fig. 17.

In Fig. 17 three regimes can be distinguished for the three less compact targets and only two for the most compact ones. At the beginning, an initial regime of constant energy is observed for the 30 first shots. During this regime the absolute value of the energy cannot be linked to the target compaction; variations may exist due to slight changes of the laser focus because of the target height and orientation. Then during the next regime the acoustic energy decreases linearly with the number of shots. It can be noted that the slope is largest for the least compact JSC1 target (2 tonnes compaction), reduces for the 3 tonnes and 4 tonnes compacted targets and is then significantly lower for the 4 last, most compact, targets. In fact, there is no longer a difference in the slope for the targets compacted by 6 to 15 tonnes. Finally, for the three first targets, a third regime can be observed following a sharp slope change. The shot number where this transition appears is higher for harder targets.

We suggest that the first constant energy regime is linked to the initial formation phase of the crater. Then, during the second regime as the energy decreases rapidly, this might indicate that the shock wave is confined deeper into the crater or that the coupling between the laser and the crater wall is reduced. In all cases, this could be indicative of the growth of the crater. The slope of this portion decreases as the compaction increases indicating that, the less compact the target is, the faster we penetrate into the sample. For the last regime, either the coupling could have reached a minimum value, or the depth no longer evolves because of the collapse of the crater wall. This change may also have occurred for the four most compacted targets if the laser had been fired a few more times. This suggested evolution of the penetration depth with the number of shots will be investigated in future studies.

5.5. Spectral analysis

The evolution of spectral content of a single LIBS shot can also be studied. The amplitude spectral density (computed using the Welch method; Welch, 1967) of the 432 shots on the 15 tonnes compacted JSC1 are represented in Fig. 18. In this figure, the spectra were estimated over a 1.3 ms long time window and are normalised with respect to the integral of the median spectrum. As mentioned in Section 4.2, the signal rises from the noise floor below 10 kHz. The typical spectrum for each shot looks similar but the intensity decreases with the number of shots. This is coherent with Fig. 17 as the energy of the time signal is equal to the integral of the corresponding spectrum (see Parseval's theorem saying that the energy of a signal is equal to the integral of the square of its transform in the frequency domain). As the intensity differences are largest in the LIBS bandwidth (around 1 kHz), each spectrum is integrated between 700 Hz and 2 kHz. The evolution of the integrated spectral densities, normalised by the mean value over the first 10 shots, is shown in Fig. 19 for the different JSC1 targets.

The variations of the integrated spectral densities with increasing shot number(Fig. 19) display the same trends as the acoustic energy results presented above (Fig. 17): a constant amplitude for the first tens of shots followed by a decrease of the spectral energy with a decreasing slope as the level of compaction of the target increases. These results indicate that, for targets with low levels of compaction (< 6 tonnes), it will be possible to differentiate between targets of different hardness using the Mars Microphone.

5.6. Application to Martian soils

It has been demonstrated above that the microphone could be used as a remote sensing tool to differentiate soils with different levels of compaction at distances up to 4 m from the SuperCam instrument aboard the Mars 2020 rover. This complementary information about the physical properties of targets will provide an additional way to retrieve the geologic context of soils.

On its way to Mount Sharp, the Mars Science Laboratory Curiosity rover spent several sols investigating the Rocknest aeolian bedform, where the scoop was first used to collect and deliver solid samples into mineralogical and chemical analysis instruments (Blake et al., 2016). The Mars Hand Lens Imager (MAHLI) took close-up pictures of the scoop trenches (Fig. 20, left) to get the morphology and the internal structure of the sand deposit. This revealed a stratification composed of a coarse grain cohesive crust on the surface followed by the superposition of armored strata and moderate fine grain cohesive sand within the interior (Minitti et al., 2013). This crucial information, that gives insights into the conditions of formation of this sand shadow, were acquired at less than 30 cm working distance.

ChemCam LIBS measurements were performed on the scuff sidewalls on Mars (Fig. 20, right). In the context of the Mars 2020/SuperCam instrument, the measure of the shock wave energy from theses 15 craters would have been useful to compare the compaction level of the different layers. During the Mars 2020 mission, the Mars Microphone acoustic measurements will be available for each SuperCam LIBS target, at distances of up to 4 m from the rover.

6. Conclusions

The SuperCam instrument suite onboard the Mars 2020 rover will include the Mars Microphone (provided by ISAE-SUPAERO in France) and will be the first microphone to record sounds from the surface of Mars. In order to record LIBS shock waves and atmospheric phenomena, the Mars Microphone must be able to record audio signals from 100 Hz to 10 kHz on the surface of Mars, with a sensitivity sufficient to monitor a LIBS shock wave at distances of up to 4 m. The Aarhus planetary simulator facility has been used to test the Mars 2020 rover microphone in a simulated Martian environment, and to verify that the SuperCam

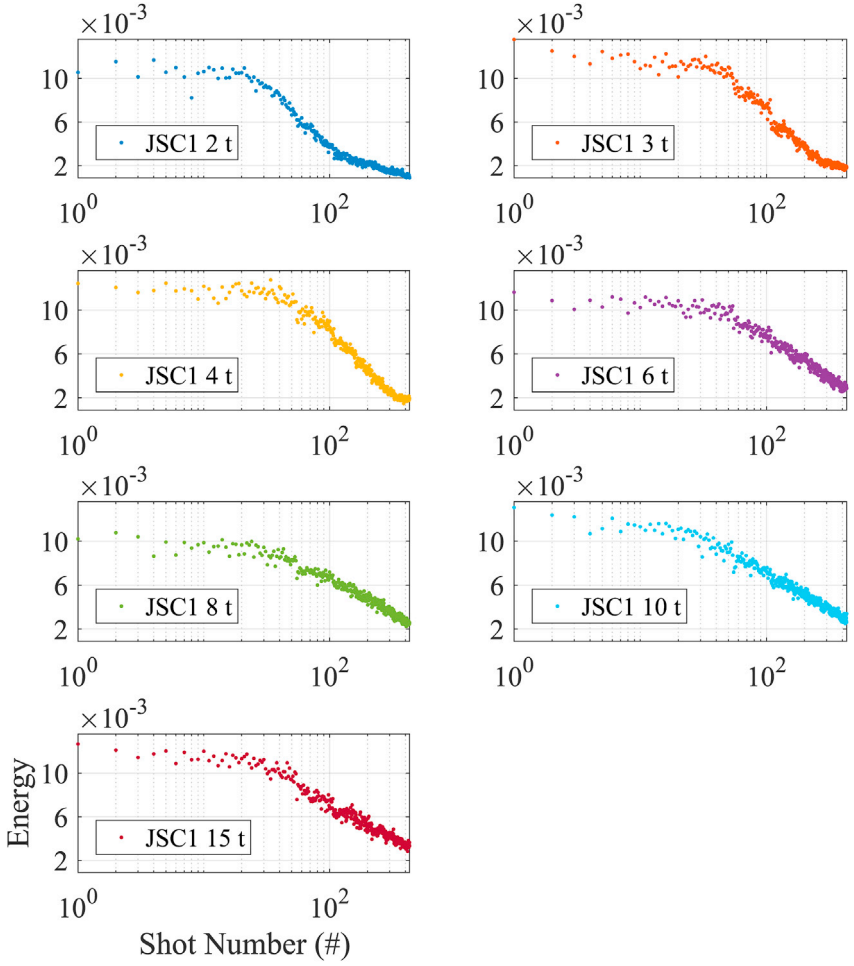

Fig. 17. Evolution of the acoustic energy during a series of 432 successive LIBS shots on the 7 compacted JSC1 targets.

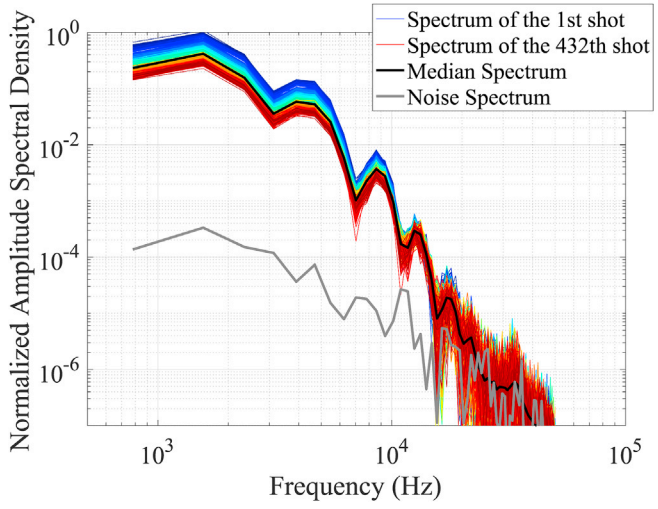

Fig. 18. Amplitude spectral densities of the acoustic signals for 432 successive LIBS shots measured by the microphone at 1.5 m from the 15 tonnes compaction JSC1 target. The black line corresponds to the median spectrum over the 432 individual spectra. The grey line shows the environmental noise spectrum in CO_2. All the spectra are normalised with respect to the integral of the median spectrum. The noise spectrum was computed over a time window of the same duration as the LIBS shot spectra (i.e., 1.3 ms).

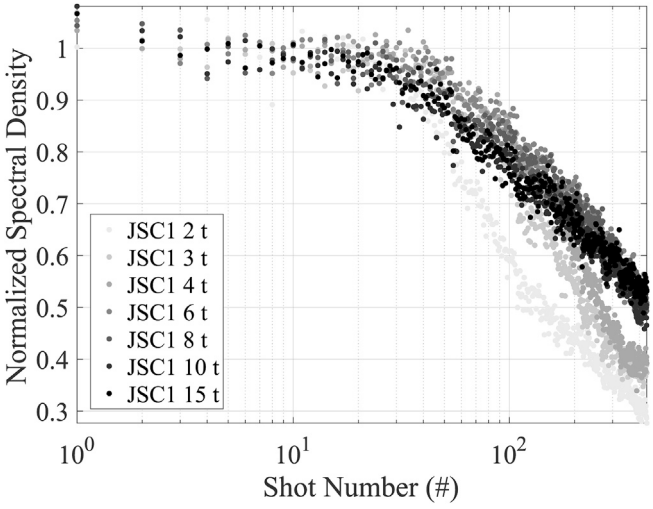

Fig. 19. Evolution of the integrated spectral density between 700 Hz and 2000 Hz during a series of 432 successive LIBS shots on the 7 compacted JSC1 targets. For each target the values are normalised by the mean value over the 10 first shots.

instrument requirements are met. The tests using an aluminium reference target have demonstrated that the acoustic signal of a laser blast is clearly recordable on the Mars Microphone in 6 mbar, CO_2 at distances of both 1.5 m and 4 m from the laser target (with a peak SNR of 40 dB and 21 dB, respectively). The presence of wind adds a high amplitude, low

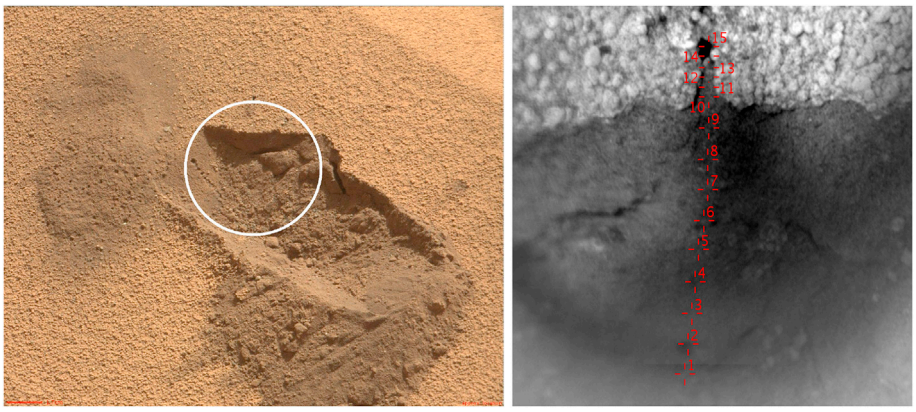

Fig. 20. Epworth3 ChemCam target at the Rocknest location. (Left) Mastcam image of the scoop trench where the target is located (white circle). (Right) Remote Micro Imager (RMI) close-up of the 15 craters made by ChemCam on the sidewalls. Images: NASA/JPL-Caltech

frequency, component to the acoustic signal. However, the wind signal can be removed with simple filtering resulting in the individual LIBS peaks being detected with a peak SNR of 28 dB at 1.5 m from the laser target and 19 dB at 4 m from the laser target. The experiments performed with the microphone at −80° C (in a CO_2 6 mbar atmosphere) and at 4 m from the laser target have demonstrated that the peak amplitude of the LIBS acoustic signal can be detected with a SNR of 26 dB. Therefore, these experimental results performed in a Martian environment have demonstrated that the SuperCam/Mars Microphone performance requirements are satisfied.

Tests in the controlled Martian environment on seven Martian soil analogue targets with an increasing hardness and level of compaction have demonstrated that the acoustic energy is indeed a reliable parameter to describe the shock wave caused by a laser blast. The acoustic energy decreases as a function of the number of LIBS shots, with a steeper decrease for the less compact targets. This supports the idea that ablation rates and thus penetration depth may be linked to the target compaction and hardness. These results indicate that similar SuperCam/Mars Microphone experiments on Mars will be able to differentiate weakly consolidated Martian soils of different compaction levels.

Acknowledgements

We gratefully acknowledge funding from the French space agency (CNES), from ISAE-SUPAERO, from Région Occitanie and from Europlanet. Europlanet 2020 RI has received funding from the European Union's Horizon 2020 research and innovation programme under grant agreement No 654208. RL acknowledges Europlanet Transnational Access program 15-EPN-008 and the support of NASA via Mars Fundamental Research Program grant NNX12AJ47G.

References

Allen, C.C., Jager, K.M., Morris, R.V., Lindstrom, D.J., Lindstrom, M.M., Lockwood, J.P., 1998. JSC MARS-1: a Martian Soil Simulant. https://doi.org/10.1061/40339(206)54.

Bass, H.E., Chambers, J.P., 2001. Absorption of sound in the martian atmosphere. J. Acoust. Soc. Am. 109 (6).

Bckle, H., 1959. Progress in micro-indentation hardness testing. Metall. Rev. 4 (1), 49–100. https://doi.org/10.1179/095066059790421746.

Blake, D.F., Morris, R.V., Kocurek, G., Morrison, S.M., Downs, R.T., Bish, D., Ming, D.W., Edgett, K.S., Rubin, D., Goetz, W., Madsen, M.B., Sullivan, R., Gellert, R., Campbell, I., Treiman, A.H., McLennan, S.M., Yen, A.S., Grotzinger, J., Vaniman, D.T., Chipera, S.J., Achilles, C.N., Rampe, E.B., Sumner, D., Meslin, P.-Y., Maurice, S., Forni, O., Gasnault, O., Fisk, M., Schmidt, M., Mahaffy, P., Leshin, L.A., Glavin, D., Steele, A., Freissinet, C., Navarro-González, R., Yingst, R.A., Kah, L.C., Bridges, N., Lewis, K.W., Bristow, T.F., Farmer, J.D., Crisp, J.A., Stolper, E.M., Des Marais, D.J., Sarrazin, P., 2013. Curiosity at gale crater, mars: characterization and analysis of the rocknest sand shadow. Science 341 (6153). https://doi.org/10.1126/science.1239505.

Chaleard, C., Mauchien, P., Andre, N., Uebbing, J., Lacour, J.L., Geertsen, C., 1997. Correction of matrix effects in quantitative elemental analysis with laser ablation optical emission spectrometry. J. Anal. At. Spectrom. 12, 183–188. https://doi.org/10.1039/A604456E.

Chen, G., Yeung, E.S., 1988. Acoustic signal as an internal standard for quantitation in laser-generated plumes. Anal. Chem. 60 (20), 2258–2263. https://doi.org/10.1021/ac00171a020.

Conesa, S., Palanco, S., Laserna, J., 2004. Acoustic and optical emission during laser-induced plasma formation. Spectrochim. Acta B Atom Spectrosc. 59 (9), 1395–1401. https://doi.org/10.1016/j.sab.2004.06.004.

Cremers, D.A., Radziemski, L.J., 2006. Handbook of Laser-induced Breakdown Spectroscopy. John Wiley & Sons, Ltd. https://doi.org/10.1002/0470093013.

Delory, G.T., Luhmann, J., Friedman, L., Betts, B., 2007. Development of the first audio microphone for use on the surface of mars. J. Acoust. Soc. Am. 121 (5) https://doi.org/10.1121/1.4782072, 3116–3116.

Diaci, J., Možina, J., 1992. Investigation of blast waves generated by laser induced damage processes. Optic Commun. 90 (1), 73–78. https://doi.org/10.1016/0030-4018(92)90331-K.

Diaci, J., Možina, J., 1992. A study of blast waveforms detected simultaneously by a microphone and a laser probe during laser ablation. Appl. Phys. A 55 (4), 352–358. https://doi.org/10.1007/BF00324084. https://doi.org/10.1007/BF00324084.

Grad, L., Možina, J., 1993. Acoustic in situ monitoring of excimer laser ablation of different ceramics. Appl. Surf. Sci. 69 (1), 370–375. https://doi.org/10.1016/0169-4332(93)90536-K.

Holstein-Rathlou, C., Merrison, J., Iversen, J.J., Jakobsen, A.B., Nicolajsen, R., Nørnberg, P., Rasmussen, K., Merlone, A., Lopardo, G., Hudson, T., Banfield, D., Portyankina, G., 2014. An environmental wind tunnel facility for testing meteorological sensor systems. J. Atmos. Ocean. Technol. 31, 447–457. https://doi.org/10.1175/JTECH-D-13-00141.1.

Hrdlika, A., Zaorlkov, L., Galiov, M., tvrtnkov, T., Kanick, V., Otruba, V., Novotn, K., Krsensk, P., Kaiser, J., Malina, R., Plenkov, K., 2009. Correlation of acoustic and optical emission signals produced at 1064 and 532 nm laser-induced breakdown spectroscopy (libs) of glazed wall tiles. Spectrochim. Acta B Atom Spectrosc. 64 (1), 74–78. https://doi.org/10.1016/j.sab.2008.10.043.

Lorenz, R.D., Merrison, J., Iversen, J.J., 2017. Wind noise and sound propagation experiments in the Aarhus mars atmosphere simulation chamber. In: Forget, F., Millour, M. (Eds.), The Mars Atmosphere: Modelling and Observation, p. 4405.

Lu, Y., Lee, Y., Hong, M., Low, T., 1997. Acoustic wave monitoring of cleaning and ablation during excimer laser interaction with copper surfaces. Appl. Surf. Sci. 199, 137–146.

Maurice, S., Wiens, R.C., Saccoccio, M., Barraclough, B., Gasnault, O., Forni, O., Mangold, N., Baratoux, D., Bender, S., Berger, G., Bernardin, J., Berthé, M., Bridges, N., Blaney, D., Bouyé, M., Caïs, P., Clark, B., Clegg, S., Cousin, A., Cremers, D., Cros, A., DeFlores, L., Derycke, C., Dingler, B., Dromart, G., Dubois, B., Dupieux, M., Durand, E., d'Uston, L., Fabre, C., Faure, B., Gaboriaud, A., Gharsa, T., Herkenhoff, K., Kan, E., Kirkland, L., Kouach, D., Lacour, J.-L., Langevin, Y., Lasue, J., Le Mouélic, S., Lescure, M., Lewin, E., Limonadi, D., Manhès, G., Mauchien, P., McKay, C., Meslin, P.-Y., Michel, Y., Miller, E., Newsom, H.E., Orttner, G., Paillet, A., Parès, L., Parot, Y., Pérez, R., Pinet, P., Poitrasson, F., Quertier, B., Sallé, B., Sotin, C., Sautter, V., Séran, H., Simmonds, J.J., Sirven, J.-B., Stiglich, R., Striebig, N., Thocaven, J.-J., Toplis, M.J., Vaniman, D., 2012. The chemcam instrument suite on the mars science laboratory (msl) rover: science objectives and mast unit description. Space Sci. Rev. 170 (1), 95–166. https://doi.org/10.1007/s11214-012-9912-2.

Maurice, S., Wiens, R.C., Anderson, R., Beyssac, O., Bonal, L., Clegg, S., DeFlores, L., Dromart, G., Fischer, W., Forni, O., Gasnault, O., Grotzinger, J., Johnson, J., Martinez-Frias, J., Mangold, N., McLennan, S., Montmessin, F., Rull, F., Sharma, S., Fouchet, T., Poulet, F., SuperCam Team, 2015. Science objectives of the SuperCam instrument for the Mars2020 rover. In: Lunar and Planetary Science Conference, Vol. 46 of Lunar and Planetary Inst. Technical Report, p. 2818.

Maurice, S., Wiens, R.C., Rapin, W., Mimoun, D., Jacob, X., Betts, B., Clegg, S., Cousin, A., Gasnault, O., Forni, O., Lasue, J., Meslin, P.-Y., Bell, J.F., Delory, G., 2016. A microphone supporting LIBS investigation on mars. In: Lunar and Planetary Science Conference, Vol. 47 of Lunar and Planetary Inst. Technical Report, p. 3044.

Maurice, S., Jacob, X., Couvert, L., Mimoun, D., Wiens, R., Rapin, W., Cousin, A., Forni, O., Gasnault, O., Lasue, J., Meslin, P.-Y., 2017. Acoustic recording of LIBS analyses in preparation for mars 2020. In: Lunar and Planetary Science Conference, Vol. 48 of Lunar and Planetary Inst. Technical Report, p. 2647.

Mimoun, D., Murdoch, N., Lognonné, P., Hurst, K., Pike, W.T., Hurley, J., Nébut, T., Banerdt, W.B., Team, S., 2017. The noise model of the seis seismometer of the insight mission to mars. Space Sci. Rev. 211. https://doi.org/10.1007/s11214-017-0409-x10.1007/s11214-017-0409-x.

Minitti, M.E., Kah, L.C., Yingst, R.A., Edgett, K.S., Anderson, R.C., Beegle, L.W., Carsten, J.L., Deen, R.G., Goetz, W., Hardgrove, C., Harker, D.E., Herkenhoff, K.E., Hurowitz, J.A., Jandura, L., Kennedy, M.R., Kocurek, G., Krezoski, G.M., Kuhn, S.R., Limonadi, D., Lipkaman, L., Madsen, M.B., Olson, T.S., Robinson, M.L., Rowland, S.K., Rubin, D.M., Seybold, C., Schieber, J., Schmidt, M., Sumner, D.Y., Tompkins, V.V., Van Beek, J.K., Van Beek, T., 2013. Mahli at the rocknest sand shadow: science and science-enabling activities. J. Geophys. Res.: Plan 118 (11), 2338–2360. https://doi.org/10.1002/2013JE004426.

Murdoch, N., Mimoun, D., Garcia, R.F., Rapin, W., Kawamura, T., Lognonné, P., Banfield, D., Banerdt, W.B., 2017. Evaluating the Wind-Induced Mechanical Noise on the InSight Seismometers. Space Sci. Rev. 211. https://doi.org/10.1007/s11214-016-0311-y.

Palanco, S., Laserna, J., 2003. Spectral analysis of the acoustic emission of laser-produced plasmas. Appl. Opt. 42 (30), 6078–6084. https://doi.org/10.1364/AO.42.006078.

Qin, Q., Attenborough, K., 2004. Characteristics and application of laser-generated acoustic shock waves in air. Appl. Acoust. 65 (4), 325–340. https://doi.org/10.1016/j.apacoust.2003.11.003.

Welch, P., 1967. The use of fast fourier transform for the estimation of power spectra: a method based on time averaging over short, modified periodograms. IEEE Trans. Audio Electroacoust. 15 (2), 70–73. https://doi.org/10.1109/TAU.1967.1161901.

Wiens, R., Maurice, S., Lasue, J., Forni, O., Anderson, R., Clegg, S., Bender, S., Blaney, D., Barraclough, B., Cousin, A., Deflores, L., Delapp, D., Dyar, M., Fabre, C., Gasnault, O., Lanza, N., Mazoyer, J., Melikechi, N., Meslin, P.-Y., Newsom, H., Ollila, A., Perez, R., Tokar, R., Vaniman, D., 2013. Pre-flight calibration and initial data processing for the chemcam laser-induced breakdown spectroscopy instrument on the mars science laboratory rover. Spectrochim. Acta B Atom Spectrosc. 82, 1–27. https://doi.org/10.1016/j.sab.2013.02.003.

Wiens, R., Maurice, S., Perez, F., 2017. The SuperCam remote sensing instrument suite for the mars 2020 rover: a preview. Spectroscopy 32 (5), 50–55.

Williams, J.-P., 2001. Acoustic environment of the Martian surface. J. Geophys. Res. 106, 5033–5042. https://doi.org/10.1029/1999JE001174.